Remote estimation of grassland gross primary production during extreme meteorological seasons

Rossini; M.; Migliavacca; M.; Galvagno; M.; Meroni; M.; Cogliati; S.; Cremonese; E.; Fava; F.; Gitelson; A.; Julitta; T.; di Cella; U.M.; Siniscalco; C.; Colombo; R.. Remote estimation of grassland gross primary production during extreme meteorological seasons. INTERNATIONAL JOURNAL OF APPLIED EARTH OBSERVATION AND GEOINFORMATION. 29 (1) pp: 1-10.
DOI: 10.1016/j.jag.2013.12.008

Remote estimation of grassland gross primary production during extreme meteorological seasons

Micol Rossini[a,], Mirco Migliavacca[b], Marta Galvagno[c], Michele Meroni[d], Sergio Cogliati[a], Edoardo Cremonese[c], Francesco Fava[a], Anatoly Gitelson[e], Tommaso Julitta[a], Umberto Morra di Cella[c], Consolata Siniscalco[f], Roberto Colombo[a]

Highlights

•Models driven by spectral and meteorological data were tested to estimate GPP.
•Best performing models are based entirely on remotely sensed data.
•Vegetation indexes related to chlorophyll explained most of the variability in GPP.
•The use of potential PAR instead of incident PAR improved GPP estimation.
•Best performing models were driven also by PRI.

Abstract

Different models driven by remotely sensed vegetation indexes (VIs) and incident photosynthetically active radiation (PAR) were developed to estimate gross primary production (GPP) in a subalpine grassland equipped with an eddy covariance flux tower. Hyperspectral reflectance was collected using an automatic system designed for high temporal frequency acquisitions for three consecutive years, including one (2011) characterized by a strong reduction of the carbon sequestration rate during the vegetative season. Models based on remotely sensed and meteorological data were used to estimate GPP, and a cross-validation approach was used to compare the predictive capabilities of different model formulations. Vegetation indexes designed to be more sensitive to chlorophyll content explained most of the variability in GPP in the ecosystem investigated, characterized by a strong seasonal dynamic. Model performances improved when including also $PAR_{potential}$ defined as the maximal value of incident PAR under clear sky conditions in model formulations. Best performing models are based entirely on remotely sensed data. This finding could contribute to the development of methods for quantifying the temporal variation of GPP also on a broader scale using current and future satellite sensors.

Keywords

- Gross primary production;
- Vegetation index;
- PRI;
- Grassland;
- Extreme events;
- Potential photosynthetically active radiation

1. Introduction

Terrestrial plants play important roles in the global carbon sequestration as they fix carbon dioxide (CO_2) as organic compounds through photosynthesis. Terrestrial gross primary production (GPP), the total amount of CO_2 fixed by terrestrial ecosystems, is one of the determinants of land-atmosphere CO_2 exchange (Beer et al., 2010). Thus, accurate GPP estimates can provide valuable information for global carbon studies. Among terrestrial ecosystems, mountain grasslands show a high interannual variability of their productivity (Yi et al., 2012). This variability is enhanced by grassland vulnerability to extreme climate events, such as unusual spring warm temperature which can contribute to early snowmelt in mountain environments (Beniston, 2005). The melting of snow cover influences the start and length of the summer growing season, the amount and timing of nutrients and water release from the snow pack and can contribute to changes in species composition (Wipf and Rixen, 2010). The expected increase of the occurrence of extreme events predicted by models and confirmed by observational data (Easterling et al., 2000 and Meehl and Tebaldi, 2004) could hamper our ability to quantify ecosystem production. Hence, the development of models able to estimate ecosystem carbon cycle related processes across years characterized by markedly different meteorological conditions is necessary to increase our confidence of future model predictions.

Measurements of vegetation reflectance at eddy covariance (EC) sites have notably increased in recent years (Balzarolo et al., 2011) because remote sensing holds considerable potential for advancing our capabilities to estimate and monitor vegetation production at different temporal and spatial scales. Several studies demonstrated the effectiveness of empirical models driven by remote sensing inputs to model GPP on different ecosystems (Peng et al., 2011 and Wu et al., 2009), including grasslands (Rossini et al., 2012). Nevertheless a general consensus about model formulations and input variables performing better, especially considering long term data series characterized by high inter-annual variability, has still to be achieved.

Previous studies reported the ability to model GPP using vegetation indexes (VIs) designed to be sensitive to chlorophyll (Chl) content. Chlorophyll content is a key variable for explaining GPP variability in vegetation characterized by strong seasonality, such as crops (Gitelson et al., 2006b, Peng et al., 2011 and Rossini et al., 2010) or grasslands (Rossini et al., 2012). This is not surprising since Chl content is a main factor controlling the amount of light absorbed by green vegetation and also directly relates to the enhanced electron transport activity, which governs light use efficiency (LUE). The accuracy in GPP estimation may be improved taking into account high frequency changes in radiation conditions and light use efficiency modulation, through the inclusion of incident photosynthetically active radiation (PAR_i) and surrogate of LUE, the photochemical reflectance index (PRI, Gamon et al., 1992) in model formulation (Peng et al., 2011, Rossini et al., 2012 and Sakamoto et al., 2011).

For the calibration of this kind of models an estimation of PAR_i is required. In the prospect of GPP monitoring from spaceborne remote sensing sensors, an accurate proxy for PAR_i that can be measured remotely is needed. Shortwave radiation obtained from coarse scale meteorological data sets from the NASA Data Assimilation Office was used as a substitute for PAR_i by Sakamoto et al. (2011). However, these estimates of PAR_i have significant uncertainties; the coefficient of variation was 23.6% and mean normalized bias was 13.9% (Sakamoto et al., 2011). Alternatively PAR_i can be indirectly estimated by radiative transfer modeling approach (e.g., Liu et al., 2008) once the optical properties of the atmosphere have been retrieved. However, incorporating such radiative transfer calculations into the practical generation of standardized product providing regular observations of global PAR_i is still a challenging topic in remote sensing (Liang et al., 2006).

Gitelson et al. (2012) suggested using potential photosynthetically active radiation ($PAR_{potential}$), defined as the maximal value of incident PAR under clear sky conditions, rather than PAR_i for estimating GPP. Such approach has the advantage that $PAR_{potential}$ can be more easily estimated using radiative transfer models or look-up table-based algorithms (Lyapustin, 2003).

To our knowledge, such approach has been successfully applied in soybean and maize using Landsat and daily MODIS satellite images (Gitelson et al., 2012 and Peng et al., 2013), but it has never been applied to simulate GPP using ground spectral reflectance measurements collected with daily resolution.

This paper provides an evaluation of the robustness of an approach based solely on remotely sensed data to estimate GPP over grasslands. We monitored spectral reflectance throughout the growth period of a subalpine grassland during three consecutive years (2009–2011), including a year (2011) characterized by the longest snow-free period on record (83 years) leading to changes in canopy structure and functioning with a strong reduction of the carbon sequestration rate during the carbon uptake period (Galvagno et al., 2013).

The specific objectives of this paper are (1) to evaluate the robustness of GPP prediction by remote sensing driven models using a three year dataset including one year with an exceptionally long growing season, (2) to assess the performance of the best model formulation, and (3) to test whether the use of $PAR_{potential}$ improves the accuracy in GPP estimation.

2. Methods

2.1. Site description and micrometeorological measurements

The study was conducted in an unmanaged grassland of the subalpine belt located in the North-Western Italian Alps (45°50′40″ N, 7°34′41″ E, Torgnon, Aosta Valley) at 2160 m a.s.l. during three growing seasons (2009–2011). The vegetation of the site is composed mainly by matgrass (*Nardus stricta*) and, secondarily, by *Trifolium alpinum*, *Arnica montana*, *Poa alpina* and *Carex sempervirens*. The area is classified as an intra-alpine region with semi-continental climate with an annual mean temperature of 3.1 °C and mean annual precipitation of about 880 mm (Mercalli and Berro, 2003). The snow-free period lasts generally from late May to early November. This site is approximately 9 ha and it is equipped with an EC flux tower which provides continuous measurements of net ecosystem CO_2 exchange (NEE) from January 2009. Detailed descriptions of the EC flux measurements, the procedures used to partition the NEE to derive GPP and of the flux footprint are reported in Migliavacca et al. (2011) and Galvagno et al. (2013). Along with EC fluxes, the main meteorological variables (in particular PAR_i) are available with a time step of 30 min.

2.2. Radiometric measurements and spectral vegetation index computation

Hyperspectral reflectance measurements were collected in the proximity of the EC tower using the HyperSpectral Irradiometer (HSI, Cogliati, 2011 and Meroni et al., 2011), designed for unattended high temporal frequency acquisitions. This instrument acquired spectra in the visible and near-infrared region (400–1000 nm) with a full width at half maximum of 1 nm.

HSI employs a rotating arm equipped with a cosine-response optic to measure alternately the sky (sensor pointing zenith) and the target irradiance (sensor pointing nadir), allowing the computation of the Bi-Hemispherical Reflectance factor (BHR, Schaepman-Strub et al., 2006). With this

configuration the 97% of the total signal comes from a cone limited by a zenith angle of 80° and the maximum contribution to the measured signal comes from zenith angles around 45°. This means that with an installation height of 3.5 m above the investigated surface, the 97% of the total signal comes from a circular ground area of 40 m diameter (Meroni et al., 2011).

Hyperspectral reflectance measurements were acquired every 5 min from sunrise to sunset during the snow-free season in 2009, 2010 and 2011. The values of the VIs used in the following analyses are means of index values calculated for each reflectance spectrum collected between 11:00 and 13:00 local solar time to minimize changes in solar angle. For more details about spectral reflectance data acquisition and preprocessing see Rossini et al. (2012).

As a first step for scaling the results of this study to current and future Earth Observation systems, the VIs considered have been defined on the basis of MODIS (Moderate Resolution Imaging Spectrometer, NASA) and OLCI (Ocean and Land Colour Instrument on board of future Sentinel-3 satellite, ESA) spectral bands. In particular, we considered the following VIs: (i) the normalized difference vegetation index (NDVI) and the photochemical reflectance index (PRI) computed from MODIS simulated data, (ii) the red-edge chlorophyll index (CI_{re}), the green chlorophyll index (CI_g), the OLCI terrestrial chlorophyll index (OTCI) and the normalized difference red-edge (NDRE), computed from OLCI simulated data (Clevers and Gitelson, 2013). Their definitions using MODIS (M) and OLCI (O) spectral bands are provided in Table 1.

Table 1.

Vegetation indexes evaluated in this study. *M* refers to the MODIS band, *O* refers to the OLCI band and R_λ refers to the reflectance factor at wavelength λ in nm.

Index	Formulation	Formulation with satellite bands	References
NDVI	$\frac{R_{858.5}-R_{645}}{R_{858.5}+R_{645}}$ R858.5−R645R858.5+R645	$\frac{M2-M1}{M2+M1}$ M2−M1M2+M1	Rouse et al. (1974)
PRI	$\frac{R_{531}-R_{551}}{R_{531}+R_{551}}$ R531−R551R531+R551	$\frac{M11-M12}{M11+M12}$ M11−M12M11+M12	Gamon et al. (1992)
CI_{re}	$\frac{R_{779}}{R_{709}}-1$ R779R709−1	$\frac{O16}{O11}-1$ O16O11−1	Gitelson et al., 2003 and Gitelson et al., 2006a
CI_g	$\frac{R_{779}}{R_{560}}-1$ R779R560−1	$\frac{O16}{O6}-1$ O16O6−1	Gitelson et al., 2003 and Gitelson et al., 2006a
OTCI	$\frac{R_{754}-R_{709}}{R_{709}-R_{681}}$ R754−R709R709−R681	$\frac{O12-O11}{O11-O10}$ O12−O11O11−O10	Dash and Curran (2004)
NDRE	$\frac{R_{754}-R_{709}}{R_{754}+R_{709}}$ R754−R709R754+R709	$\frac{O12-O11}{O12+O11}$ O12−O11O12+O11	Gitelson and Merzlyak (1994)

2.3. Data selection

Ground-observed PAR_i values were used to calculate $PAR_{potential}$ as the maximal PAR_i in 8-day-PAR_i windows (Gitelson et al., 2012 and Peng et al., 2013). The relationship between maximal PAR_i and the day of the year (DOY) was fitted with polynomial functions to compute $PAR_{potential}$ at daily step. The best-fit functions, a second and a third order polynomial, were used to calculate midday and daily $PAR_{potential}$ respectively. Based on $PAR_{potential}$, the frequency of occurrence of cloudy or hazy weather conditions during the three years was then computed as the percentage difference $(PAR_{potential} - PAR_i)/PAR_{potential}$ (hereafter ΔPAR) for each sampling date.

The proposed models were calibrated and validated using data collected with ΔPAR lower than 60%. This threshold was indicated by Peng et al. (2013) as the one for which the GPP estimation model with $PAR_{potential}$ was more accurate than the models with PAR_i.

2.4. Model development

The set of models proposed in Rossini et al. (2012) was used to estimate both the daily midday average GPP (GPP_m, μmol CO_2 m^{-2} s^{-1}) and the daily cumulated GPP (GPP_d, gC m^{-2} d^{-1}). The use of both PAR_i and $PAR_{potential}$ was tested in the following model formulations:

(i)model 1 (MOD 1), linear relationship between GPP and a VI related to canopy Chl content

equation(1)

$GPP=a_0\ VI+b_0$GPP=a0 VI+b0

(ii)model 2 (MOD 2), linear relationship between GPP and the product of a VI related to canopy Chl content and PAR

equation(2)

$GPP=a_1(VI\times PAR)+b_1$GPP=a1(VI×PAR)+b1

(iii)model 3 (MOD 3), LUE-like model (Monteith, 1972 and Monteith, 1977) assuming constant light use efficiency (ε) and modeling *f*APAR as a linear function of a VI related to canopy Chl content

equation(3)

$GPP=\varepsilon\times(a_2\ VI+b_2)\times PAR=(a_3\ VI+b_3)\times PAR$GPP=ε×(a2 VI+b2)×PAR=(a3 VI+b3)×PAR

(iv)model 4 (MOD 4), modeling ε and *f*APAR as a linear function of PRI and VI, respectively

equation(4)

$GPP=(a_4\ PRI+b_4)\times(a_5\ VI+b_5)\times PAR$GPP=(a4 PRI+b4)×(a5 VI+b5)×PAR

Model coefficients (a_x and b_x) were estimated using the Gauss-Newton nonlinear least square optimization method (Bates and Watts, 1988), implemented in the function optim() of the R standard package (R, version 2.6.2, R Development Core Team, 2011). Model accuracy was evaluated in terms of root mean square deviation (RMSD) which represents the "mean" deviation of modeled values (GPP^{mod}) with respect to the observed ones (GPP^{obs}), in the same units as the model variable under evaluation (GPP_d or GPP_m) and the relative RMSD (rRMSD, %) computed as:

equation(5)

$$\gamma rRMSD = \sqrt{\frac{1}{n}\sum_{i=1}^{n}\frac{(GPP_i^{mod} - GPP_i^{obs})^2}{(GPP_i^{obs})^2}} \times 100$$

γrRMSD=1n∑i=1n(GPPimod−GPPiobs)2(GPPiobs)2×100

where *n* is the number of samples.

When using observed PAR, models were tested using the average of the values measured between 11:00 and 13:00 local solar time for the midday analysis (μmol m^{-2} s^{-1}) and the sums of half-hourly measurements during the day (when global radiation exceeds 15 Watt m^{-2}) for the daily analysis.

Out of sample performances were assessed following a training/validation splitting approach: one year at a time was excluded using the remaining subset as the training set and the excluded one as the validation set. The model was fitted against each training set and the resulting parameterization was used to predict the CO_2 uptake of the excluded year.

3. Results and discussion

3.1. Interannual variability of gross primary production

The seasonal variations of carbon fluxes exhibited similar dynamics in 2009 and 2010 that are markedly different from 2011 (Fig. 1). The year 2011 was characterized by the earliest snowmelt since 1945 and the longest snow-free period on record (83 years) (Galvagno et al., 2013). An early snowmelt meant a lengthened snow-free period and consequently an expanded growing season for the plants. The snow-free period varied from 159 and 160 days in 2010 and 2009, respectively, to 234 days in 2011.

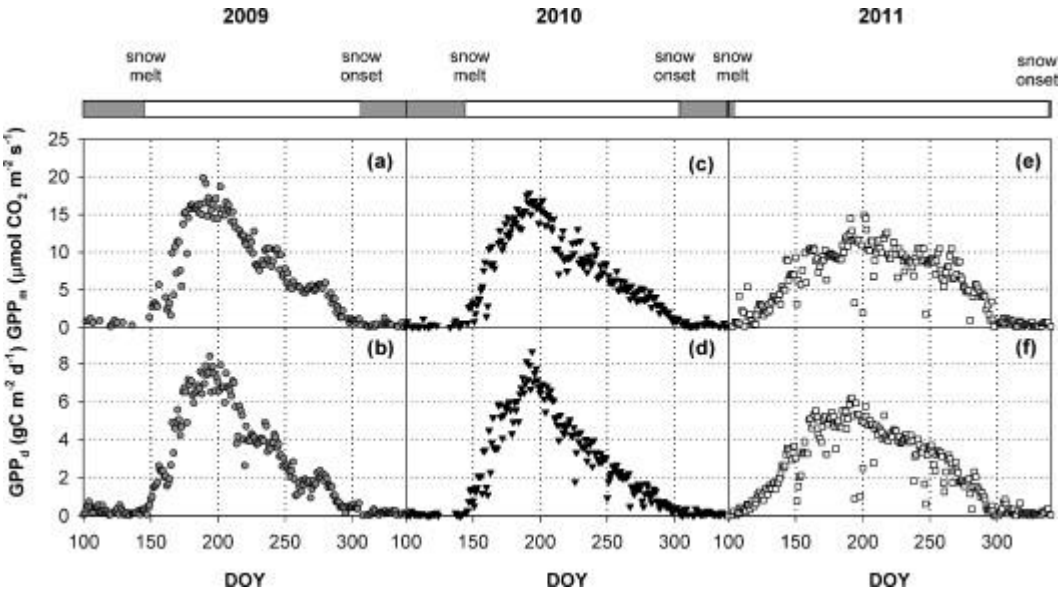

Fig. 1.

Seasonal variation of 2009 (gray circles), 2010 (black triangles) and 2011 (white squares): (a, c, e) midday Gross Primary Production (GPP_m, μmol CO_2 m^{-2} s^{-1}) and (b, d, f) daily Gross Primary Production (GPP_d, gC m^{-2} d^{-1}). DOY is day of the year.

GPP increased sharply just after snowmelt in 2009 and 2010, reaching its maximum value in mid-July (18th–13th, DOY 199 and 194). During the second part of the season the decrease rate of GPP

was slower compared to the increase one. On the contrary, in 2011 GPP increased earlier in spring, but with a lower rate and showing a less pronounced asymmetry between increasing and decreasing phases. This resulted in a longer carbon uptake period characterized by a reduced carbon sequestration rate, compared to previous years, but a similar seasonal cumulative carbon uptake (Galvagno et al., 2013).

GPP_m appeared more affected than GPP_d by the early snowmelt occurred in 2011. The peak of GPP_m in 2011 was 25% and 29% lower than those recorded in 2009 and 2010, respectively. The correspondent decrease in 2011 GPP_d peak was 16.8 and 16.6% referred to 2009 and 2010, respectively. The snowmelt timing observed in 2011 exposed plants acclimated to a narrow range of environmental conditions typical of late spring/early summer, to the unusual weather conditions of the early spring. As a result, vegetation grown in 2011 manifested, throughout the whole summer, a reduced responsiveness to high irradiance, typical of central hours of the day in this site. As GPP_d integrates periods of high and low PAR_i, the reduced responsiveness of GPP to high PAR_i is likely to be masked when considering GPP_d (Turner et al., 2003).

3.2. Time courses of spectral vegetation indexes

The seasonal variations in midday VIs are shown in Fig. 2. All VIs exhibited a clear seasonal trajectory, increasing from the end of May (DOY 160) due to canopy greening, reaching a peak in July (DOY 220) and decreasing more or less steeply afterwards with senescence and canopy yellowing. Most VIs peaked in the middle of July, except PRI which peaked about two weeks later. A possible explanation of this delay is that PRI uses bands in the green region of the spectrum where Chl absorption is weaker compared to the red region and the tendency toward saturation for medium to high canopy greenness is reduced.

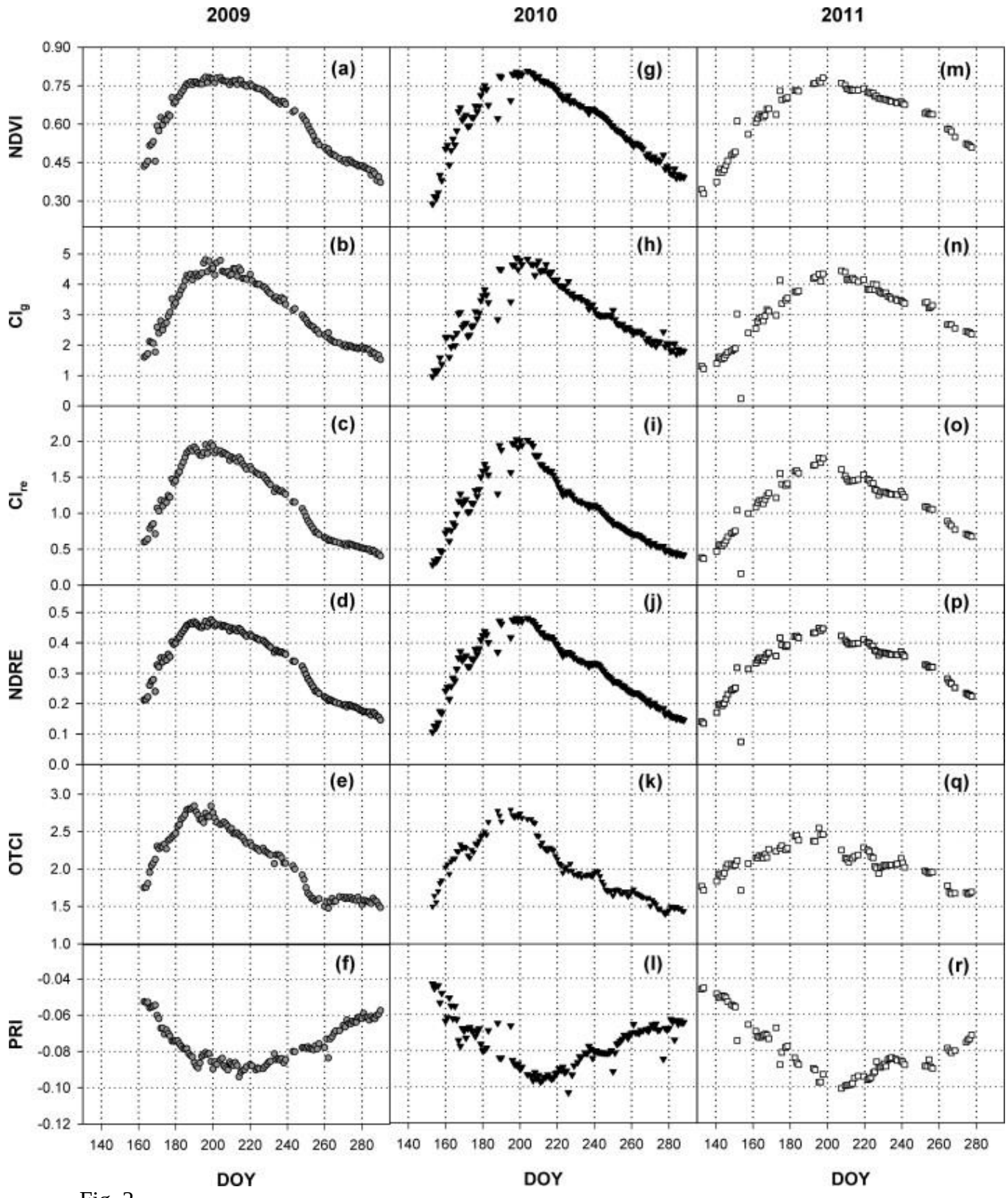

Fig. 2.

Seasonal temporal profiles of measured vegetation indexes in 2009 (circles, left panels), 2010 (triangles, middle panels) and 2011 (squares, right panels): (a, g, m) normalized difference vegetation index, NDVI; (b, h, n) green chlorophyll index, CI_g; (c, i, o) red-edge chlorophyll index, $CI_{red\text{-}edge}$; (d, j, p) normalized difference red-edge, NDRE; (e, k, q) OLCI terrestrial chlorophyll index, OTCI; (f, l, r) photochemical reflectance index, PRI. Each

point indicates the average value between 11:00 and 13:00 (local solar time). DOY is day of the year.

Comparing the three years analyzed in this study, the onset of greening was anticipated in 2011 due to the earlier snowmelt and all VIs started to increase (decrease) about 15 days earlier than the previous years. For example, NDVI level of 0.5 was attained on DOY 166, 164 and 151 in 2009, 2010 and 2011, respectively. However, the slope of the VIs in the green-up phase was lower in 2011 and VIs peaked in the same period across the three years, indicating a slower green-up period with advanced snowmelt. The maximum values reached by the VIs in 2011 were lower than those of previous years; this reduction is more evident when considering VIs computed using red-edge bands and in particular OTCI (maximum values of 2.84, 2.79 and 2.55 in 2009, 2010 and 2011, respectively). NDVI showed the most similar trends between the three years because of its saturation at medium to high canopy biomass (Huete et al., 2002). Conversely, the minimum PRI values were slightly lower in 2011.

The differences in 2011 VIs can be attributed to the response of the ecosystem to an exceptionally early snowmelt followed by cold temperature typical of springtime. This event caused a change in the typical trajectory of canopy development and physiological responses (Galvagno et al., 2013) visible also in the VI trajectories.

The examination of the seasonal time courses of the different VIs with respect to GPP showed that there was a good general correspondence between GPP and VIs tracking canopy greenness and in particular canopy Chl content: both GPP and VIs showed a more symmetric behavior between increasing and decreasing phases as well as lower peak values in 2011 compared to previous years.

3.3. Analysis of the effect of the illumination conditions

Fig. 3 shows higher occurrences of "not clear sky" conditions in 2010, with 15% of data collected with ΔPAR greater than 60%. This frequency is higher than those recorded in 2009 (7%) and 2011 (8%).

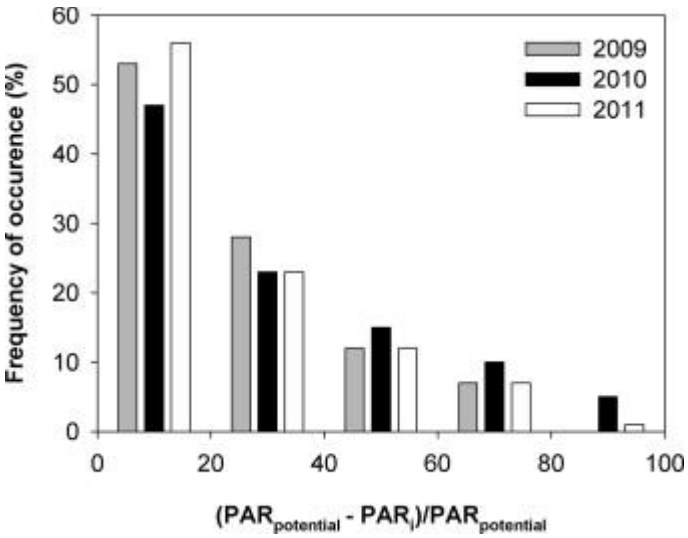

Fig. 3.

Distribution of the sampling days used in the analysis in 5 classes of $(PAR_{potential} - PAR_i)/PAR_{potential}$: from ΔPAR between 0% and 20% (clear sky conditions) to ΔPAR between 80% and 100% (overcast conditions). The percentage of days belonging to each class is plotted for each year.

The effect of including cloudy or hazy weather observations in the analysis was evaluated plotting the rRMSD of the models aimed at GPP estimation versus the maximum value of ΔPAR used as a criterion to select the observations composing both the calibration and the validation datasets. In this paragraph results obtained for GPP_d estimation in 2010 are presented as an example, as 2010 was the year characterized by higher values of ΔPAR. Fig. 4 shows that, as expected, the accuracy of all the proposed models increased as ΔPAR decreased. Higher improvements in model performances were observed between the rRMSD calculated using the complete dataset and the rRMSD computed using data collected with ΔPAR below 60%. This 60% threshold was selected as further reduction of this threshold did not result in significant performance increases. The same threshold was obtained by Peng et al. (2013) for GPP modeling in soybean and maize. Relative RMSD for models driven by $PAR_{potential}$ varied between 36% and 84% using the complete dataset and between 16% and 52% when using observations with ΔPAR < 60%. Similar improvements were observed applying the ΔPAR threshold on PAR_i: the rRMSD range varied from 29–83% to 16–52%. Models using $PAR_{potential}$ had smaller rRMSD than models using PAR_i when ΔPAR was below 80%.

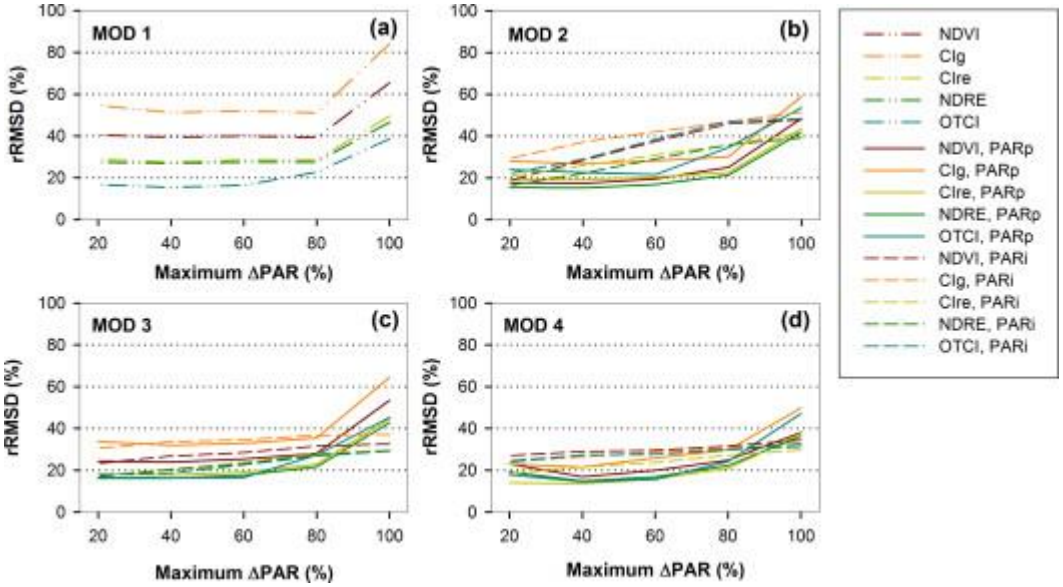

Fig. 4.

Relative root mean squared difference (rRMSD) of different GPP_d estimation models plotted versus the difference $(PAR_{potential} - PAR_i)/PAR_{potential}$ (ΔPAR, %). Results obtained for GPP_d estimation in 2010 are shown.

The analysis on midday values showed smaller improvements when considering lower ΔPAR compared to the analysis on daily values (data not shown). We hypothesize that GPP_d estimation can be more affected by variations in ΔPAR because daily GPP and PAR result from the integration of half-hourly measurements during the day. A high correlation between midday fluxes and daily fluxes (r = 0.95) enabled the daily analysis to work well when using midday remote sensing acquisitions. However, these relationships can be lowered when observations collected with highly variable weather conditions during the day are included because they may cause a decrease in the correlation between daily and midday fluxes, and consequently between daily fluxes and midday VIs. This is most likely to happen during hazy or cloudy days that can be filtered out based on ΔPAR thresholds. The proposed models were consequently calibrated and validated using only data collected with ΔPAR lower than 60%.

3.4. GPP estimation

The performances of different models for GPP_d and GPP_m estimation are shown in terms of cross validated rRMSD (Fig. 5).

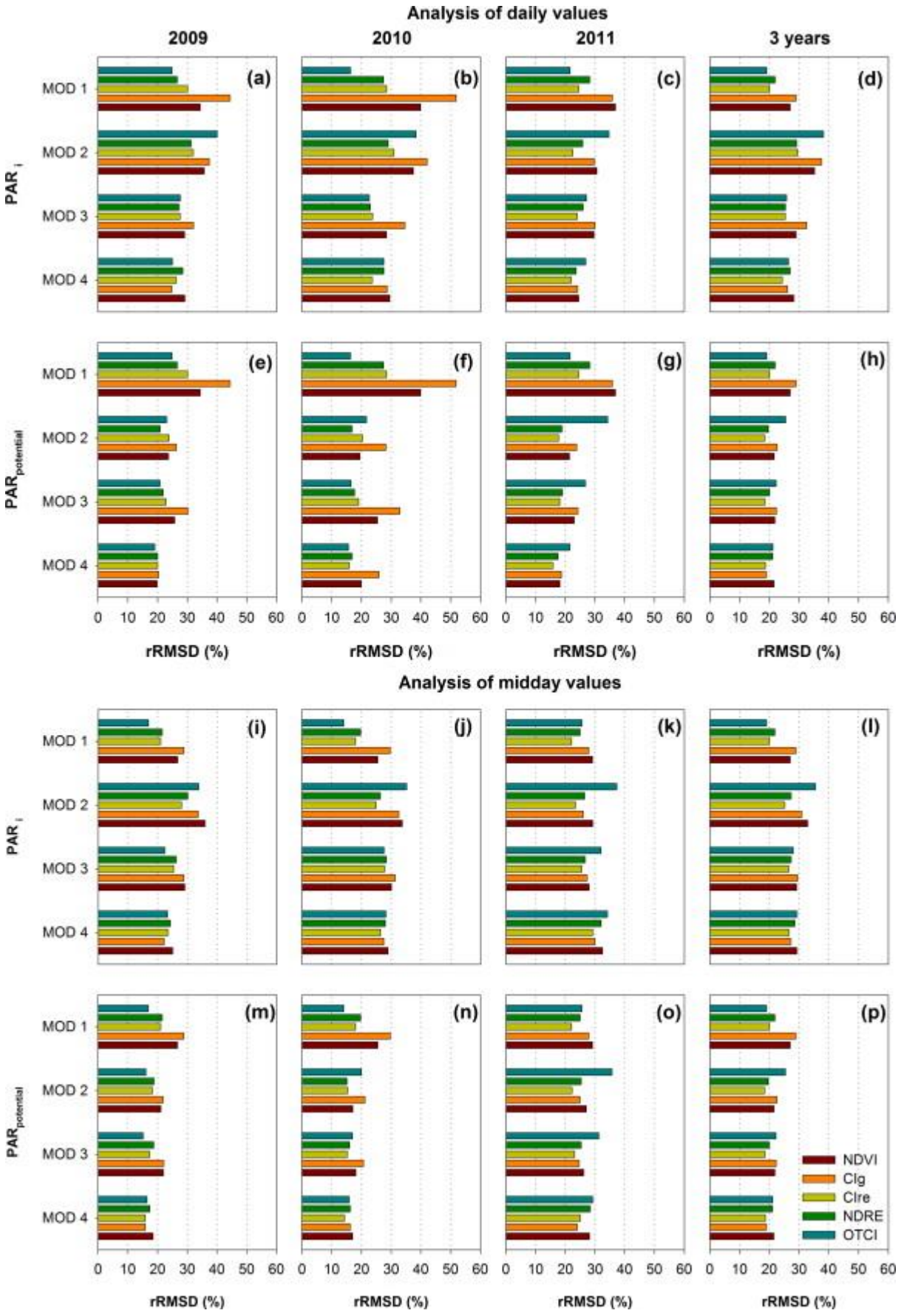
Analysis of daily values
2009
2010
2011
3 years
(a)
(b)
(c)
(d)
(e)
(f)
(g)
(h)
MOD 1
MOD 2
MOD 3
MOD 4
PAR i
PAR potential
0 10 20 30 40 50 60
rRMSD (%)
Analysis of midday values
(i)
(j)
(k)
(l)
(m)
(n)
(o)
(p)
NDVI
Clg
Clre
NDRE
OTCI

Fig. 5.

Relative root mean square deviation (rRMSD, %) between predicted and observed values using the 2009, 2010, 2011 and the total datasets for: (a–d) GPP_d estimation using PAR_i, (e–h) GPP_d estimation using $PAR_{potential}$, (i–l) GPP_m estimation using PAR_i, (m–p) GPP_m estimation using $PAR_{potential}$.

Considering the analysis of daily values, some general considerations can be drawn: (i) the VIs based on the red-edge region performed better than NDVI and CI_g; (ii) GPP estimation accuracies increased using models accounting for variations in the incident PAR (both PAR_i and $PAR_{potential}$) and including the PRI in model formulation (MOD 4); (iii) the use of $PAR_{potential}$ instead of PAR_i improved GPP estimation. The best performing model formulations allowed GPP_d estimation with a RMSD of 0.50 gC m^{-2} d^{-1} (corresponding to a rRMSD of about 15%). For most of the models, better performances were achieved using midday values. The lowest rRMSD values were confirmed at about 15% with MOD 4 driven by VIs based on red-edge wavelengths (e.g. CI_{re}). Comparing results obtained in the three years analyzed, the lowest performances in GPP_m estimation were observed in 2011. A specific discussion about the possible reasons of this is reported in the next paragraph.

Fig. 5(d, h, l, p) shows the rRMSD between predicted and observed values for GPP_m and GPP_d considering the three years together. The best performing model for GPP_m estimation is MOD 2 driven by the product of CI_{re} and $PAR_{potential}$ and MOD4 driven by CI_{re}, $PAR_{potential}$ and PRI for GPP_d estimation. This means that the use of a VI related to Chl content in combination with $PAR_{potential}$ alone or with PRI allowed to account for both the seasonal change in Chl and the modulation of GPP due to changes in radiation conditions and light use efficiency.

Models driven by $PAR_{potential}$ performed better than those driven by PAR_i. This indicates that the use of $PAR_{potential}$ improved the accuracy in GPP estimation when a decrease in PAR_i may not correspond to a decrease in GPP due to the tendency toward saturation of the relationship between GPP and PAR_i. Thus, at high irradiance loads slightly PAR_i fluctuations due to unstable weather conditions may cause noise and unpredictable uncertainties in GPP estimation. As our results show, the use of $PAR_{potential}$ in the model may partially reduce such noise of the model.

Vegetation indexes based on the red-edge region (OTCI, CI_{re} and NDRE) and designed to be sensitive to Chl content explained most of the variability in GPP and performed better than NDVI and CI_g. CI_{re} was the best performing VI when used together with PRI and PAR (MOD 4) or PAR alone (MOD 2 and MOD3) because together they account for both the seasonal change in Chl content and the modulation of GPP due to changes in radiation conditions (Peng et al., 2011). OTCI was instead the best performing index when used as single driver for GPP estimation. The use of OTCI as a single variable to predict GPP_d was already proven successful in sites dominated by a predictable seasonal cycle such as deciduous forests and grasslands (Harris and Dash, 2010). Further works are needed to evaluate the possibility to apply this approach also on vegetation characterized by weak seasonality (e.g. evergreen forests).

Although the NDVI is the most widely used spectral index at European EC sites (87.5% of the sites according to Balzarolo et al. (2011)), it exhibits limitations in GPP estimation in the investigated grassland. Models driven by NDVI alone or NDVI and PAR underestimated GPP at the beginning of the growing season (green-up phase) while overestimated GPP from DOY 180 on (data not shown). One possible reason is that NDVI response saturates with high biomass amount (Fava et al., 2010). The inclusion of PRI in model formulations improves GPP estimation using NDVI. Thus, while NDVI can provide useful information about the temporal evolution of ecosystem phenology (Hmimina et al., 2013), the potential of using NDVI for GPP monitoring requires further investigations. Fig. 6 shows the strong relationship between PRI and indexes tracking canopy Chl

content such as OTCI and CI_{re}. This relationship showed pronounced hysteresis: for the same OTCI or CI_{re}, sPRI in the green-up stage was much higher than in the senescence stage. The hysteresis was more pronounced for OTCI compared to CI_{re}. The reason of this hysteresis can be explained considering that PRI is related to the carotenoid/Chl ratio (Panigada et al., 2009 and Stylinski et al., 2002) since it measures the relative reflectance on either side of the green hump, one side being affected only by Chl absorbance and the other by the coupled Chl and carotenoid absorbance (Sims and Gamon, 2002). Carotenoid concentration increases together with Chl concentration in the green-up period while during senescence Chl decreases sharper compared to carotenoids that are retained for photoprotection (Merzlyak and Gitelson, 1995). Even if only few authors (Sims and Gamon, 2002 and Stylinski et al., 2002) reported similar relationships, PRI variation over weeks or months may be a combined function of the variation of ε and changes in the total pools of pigments. This may help explaining why the use of PRI in model formulation increases the accuracy in GPP estimation, since varying carotenoid/Chl ratios can covary with xanthophyll pigment levels, and this may enhance the ability of PRI to predict ε. On the other hand, to the extent that pigment ratios are not closely related to ε, changing pigment ratios would be a confounding variable. Thus, PRI may still be effective as a measure of changes in ε to the extent that ε is correlated with pigment content. Such a relationship appears likely in the present study but the implications of this relationship for the use of PRI in ε estimation needs to be investigated in a wider number of ecosystems.

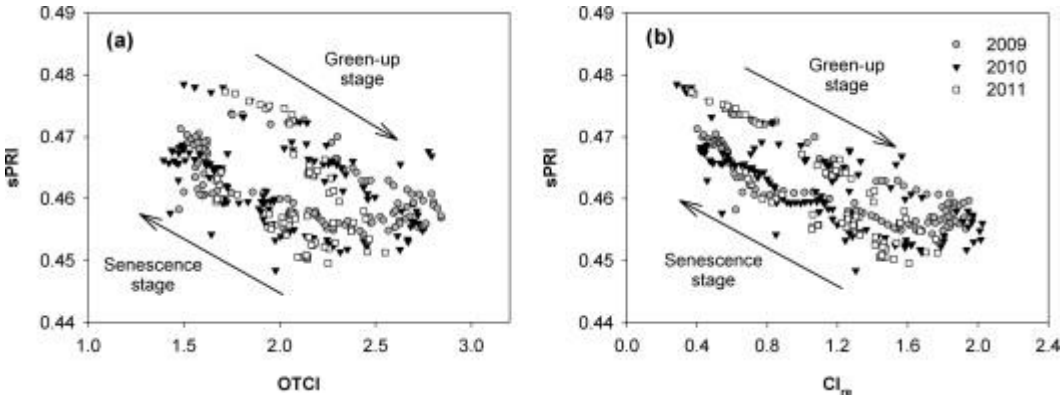

Fig. 6.

Relationship between (a) PRI and OTCI and (b) PRI and CI_{re}. PRI is plotted as scaled PRI, computed as sPRI = (PRI + 1)/2, for clarity of representation.

The modeling approach proposed here has some potential for application with current and future satellite data because all the input variables can be in principle derived from satellite observations, including $PAR_{potential}$ that can be more easily computed with radiative transfer models as compared to PAR_i. However, when working with satellite instruments, the spatial and temporal detail would be necessarily reduced compared to the one available for this study. As a result, GPP estimation uncertainty expected to be substantially greater than that achieved in this study using ground measurements. Satellite application is expected to be particularly challenging in ecosystems characterized by high spatial and temporal heterogeneity such as the one investigated here. In particular, one of the main limitations in mountain areas is that the ecosystem size is often lower than the pixel size (from 250 m to 1 km for MODIS sensor and 300 m for OLCI) causing different land cover classes to be included in the same pixel and decreasing the performances in GPP estimation.

3.5. Model performances in a year characterized by an unusually long growing season

The proposed method was tested to assess the ability in estimating GPP for the year 2011 characterized by a markedly different carbon sequestration dynamic during the vegetative season due to an extremely long growing season caused by an exceptionally early snowmelt. The prediction accuracy was better for daily rather than midday GPP. For the analysis of daily values, better results have been obtained with MOD 4 driven by $PAR_{potential}$, CI_{re} and PRI. This model yielded a RMSD of 0.55 gC m^{-2} d^{-1}, corresponding to a rRMSD of 15.8%. When analyzing midday values, MOD 1 driven by CI_{re} predicted GPP_m with the highest performances, rRMSD of 22.1%, corresponding to an absolute RMSD of 1.9 µmol CO_2 m^{-2} s^{-1}. To get a better understanding of the capability of remote sensing driven models to represent the seasonal time courses of GPP, we compared CO_2 uptake observations and model outputs obtained with the best-performing model for the daily and midday values (Fig. 7).

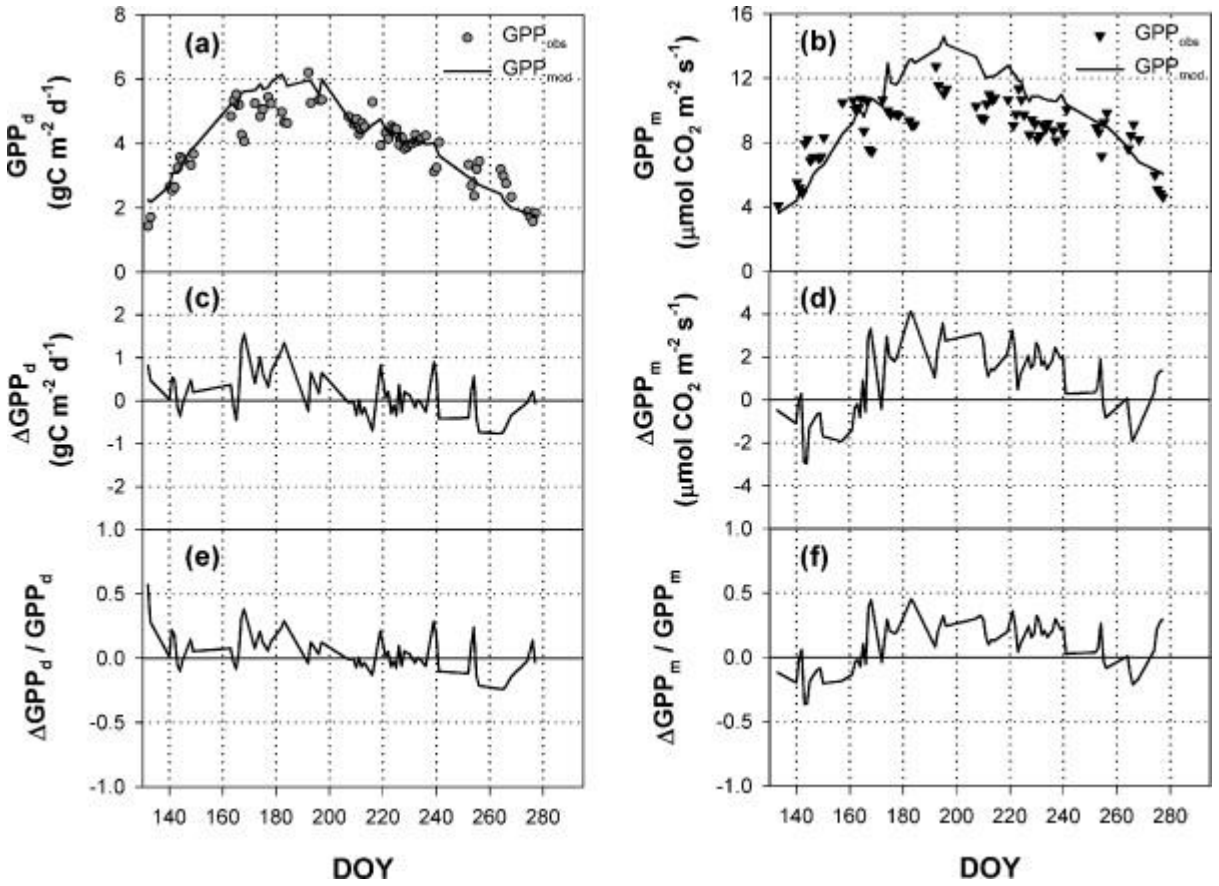

Fig. 7.

Time courses of 2011 (a) daily (gC m^{-2} d^{-1}) and (b) midday GPP (µmol CO_2 m^{-2} s^{-1}) estimated from eddy covariance measurements (GPP_{obs}) (full symbols) and GPP modeled (black line) with the best performing model formulation (GPP_{mod}): model 4 parameterized with PRI, CI_{re} and $PAR_{potential}$ (rRMSD = 15.8%) for the daily analysis and model 1 parameterized with CI_{re} (rRMSD = 22.1%) for the midday analysis. Temporal changes in the difference between simulated and observed GPP for the (c) daily (ΔGPP_d) and (d) midday (ΔGPP_m) analysis. Temporal changes in ΔGPP normalized by GPP_{obs} for the (e) daily ($\Delta GPP_d/GPP_d$) and (f) midday ($\Delta GPP_m/GPP_m$) analysis.

Predicted GPP_d values agreed quite well with observations as concerns both amplitude and seasonal phase and successfully described the dynamics captured by CO_2 uptake fluxes. Predicted GPP_m values agreed quite well with GPP_{obs} as concerns the seasonal phase but showed overestimation in the middle of the growing season (see Fig. 7d from DOY 174 to DOY 254).

The early start of season triggered by snow melting exposed plants to weather conditions harder than previous years. High altitude plants depend on highly efficient carbon assimilation since their growing season is usually very short and characterized by extreme climatic conditions (Streb et al., 1998). The acclimation of physiological processes is therefore essential to cope with such climatic conditions. The snowmelt observed in 2011 was the third earliest in the last 83 years and hence exposed the investigated grassland to less favorable weather occurring earlier in the season. Plants responded to such conditions through a reduction of the parameters describing the light response curve of photosynthesis (Galvagno et al., 2013): this means that for a given irradiance level the observed GPP was lower in 2011 compared to other years. This effect is enhanced for high irradiance loads occurring at noon. As a consequence when the models were used to predict GPP_m, predicted GPP_m was overestimated because the models were trained with the 2009 and 2010 datasets characterized by higher GPP_m values for the same PAR_i. It is interesting to note that, despite the extraordinary conditions experienced in 2011, the proposed method allowed to accommodate for inter-annual changes in the length of the growing season and predict GPP_d and GPP_m with an acceptable accuracy. Since future warming of the Alpine region (Foppa and Seiz, 2012) will likely result in earlier snowmelt dates and thus an increase of the frequency of events such the one occurred in 2011, the evaluation of the robustness of models proposed for GPP estimation in such conditions is crucial.

This study demonstrates the importance to collect spectral reflectance data continuously, regularly and from a worldwide network in connection with the well-established network of flux towers (FLUXNET) to improve our ability to model changes in ecosystem production in response to interannual climatic variations.

4. Conclusions

This study showed that models entirely based on remote-sensing data can provide good predictions of GPP in high altitude grassland ecosystems. Better results in GPP_m have been obtained using the model driven by the product of CI_{re} and $PAR_{potential}$, while accuracy in GPP_d estimation have been obtained with the model driven by CI_{re}, $PAR_{potential}$ and PRI, confirming the highest performances of VIs related to Chl content for GPP estimation. However, the use of PRI as estimate of ε over weeks or months should be carefully evaluated because at this temporal scale PRI may be a combined function of changes in ε and changes in chlorophyll content as well as carotenoid/Chl ratio. So PRI is expected to provide good estimate of ε to the extent that ε is correlated with pigment variations. Further studies are needed to explore the seasonal relationship between PRI and ε in ecosystems characterized by weak seasonal variations where the correlation between pigment seasonal variation and ε is likely to be lower.

After the application of a cloud screening criterion based on the difference between PAR_i and $PAR_{potential}$ ($\Delta PAR < 60\%$), models driven by PAR in the form of $PAR_{potential}$ provided better estimates of both GPP_m and GPP_d compared to the models driven by PAR_i. Since $PAR_{potential}$ is expected to be more easily available than PAR_i, the use of $PAR_{potential}$ can be preferred in GPP monitoring using solely remotely sensed data.

The proposed technique was validated also during a year (2011) characterized by a strong reduction of the carbon sequestration rate during the vegetative season. Results showed accurate GPP_d

estimation with a rRMSD of 15.8%, while GPP_m was estimated with a worse accuracy compared to the other years analyzed. This can be explained by the reduction of the parameters describing the light response of photosynthesis occurred in 2011 due to the unusual early snowmelt, affecting GPP_m to a higher extent compared to GPP_d. As a consequence, models calibrated with the 2009 and 2010 datasets overestimated the GPP_m measured in 2011.

Long-term time series of hyperspectral reflectance at daily resolution are available in a limited number of sites due to high costs and complexity in making the instruments running unattended. This makes difficult to test the proposed approach on similar data collected in different vegetation types. However the approach presented in this study is not limited to estimate GPP using spectral reflectance collected by radiometers mounted on a platform close to the canopy. It could be also applied to remotely sensed data collected at multiple scales from close range to satellite platforms, allowing regional or global GPP monitoring. However the large scale difference between medium to coarse resolution satellite data and in situ local hyperspectral measurements can make the direct extrapolation of this approach to wider area challenging when a single pixel contains multiple land cover classes (characterized by different VIs-GPP relationships), as in mountain areas with high landscape fragmentation and heterogeneity. Consequently, it appears worthwhile to address further research to test this kind of approach in different vegetation types using satellite-derived VIs and $PAR_{potential}$ calculation using radiative transfer approaches.

Acknowledgements

This study was supported by the PhenoALP project, an Interreg project co-funded by the European Regional Development Fund, under the operational program for territorial cooperation Italy-France (ALCOTRA) 2007–2013. The authors acknowledge the staff of the Remote Sensing of Environmental Dynamics Laboratory (DISAT, UNIMIB) for the support during field campaigns.

References

M. Balzarolo, K. Anderson, C. Nichol, M. Rossini, L. Vescovo, N. Arriga, *et al.* Ground-based optical measurements at European flux sites: a review of methods, instruments and current controversies Sensors, 11 (2011), pp. 7954–7981

D.M. Bates, D.G. Watts Nonlinear regression analysis and its applications John Wiley & Sons, New York (1988)

C. Beer, M. Reichstein, E. Tomelleri, P. Ciais, M. Jung, N. Carvalhais, *et al.* Terrestrial gross carbon dioxide uptake: global distribution and covariation with climate Science, 329 (2010), pp. 834–838

M. Beniston Mountain climates and climatic change: an overview of processes focusing on the European Alps Pure and Applied Geophysics, 162 (2005), pp. 1587–1606

J.G.P.W. Clevers, A.A. Gitelson Remote estimation of crop and grass chlorophyll and nitrogen content using red-edge bands on Sentinel-2 and -3 International Journal of Applied Earth Observation and Geoinformation, 23 (2013), pp. 344–351

S. Cogliati Development of automatic spectrometric systems for proximal sensing of photosynthetic activity of vegetation University of Milano-Bicocca (2011), p. 162

J. Dash, P.J. Curran The MERIS terrestrial chlorophyll index International Journal of Remote Sensing, 25 (2004), pp. 5403–5413

D.R. Easterling, G.A. Meehl, C. Parmesan, S.A. Changnon, T.R. Karl, L.O. Mearns Climate extremes: observations, modeling, and impacts Science, 289 (2000), pp. 2068–2074

F. Fava, G. Parolo, R. Colombo, F. Gusmeroli, G. Della Marianna, A.T. Monteiro, *et al.* Fine-scale assessment of hay meadow productivity and plant diversity in the European Alps using field spectrometric data Agriculture Ecosystems & Environment, 137 (2010), pp. 151–157

N. Foppa, G. Seiz Inter-annual variations of snow days over Switzerland from 2000–2010 derived from MODIS satellite data Cryosphere, 6 (2012), pp. 331–342

M. Galvagno, G. Wohlfahrt, E. Cremonese, M. Rossini, R. Colombo, G. Filippa, *et al.* Phenology and carbon dioxide source/sink strength of a subalpine grassland in response to an exceptionally short snow season Environmental Research Letters, 8 (2013), p. 025008

J.A. Gamon, J. Peñuelas, C.B. Field A narrow-waveband spectral index that tracks diurnal changes in photosynthetic efficiency Remote Sensing of Environment, 41 (1992), pp. 35–44

A.A. Gitelson, Y. Gritz, M.N. Merzlyak Relationships between leaf chlorophyll content and spectral reflectance and algorithms for non-destructive chlorophyll assessment in higher plant leaves Journal of Plant Physiology, 160 (2003), pp. 271–282

A.A. Gitelson, G.P. Keydan, M.N. Merzlyak Three-band model for noninvasive estimation of chlorophyll, carotenoids, and anthocyanin contents in higher plant leaves Geophysical Research Letters, 33 (2006) L11402

A. Gitelson, M.N. Merzlyak Spectral reflectance changes associated with autumn senescence of *Aesculus hippocastanum* L and *Acer platanoides* L leaves – spectral features and relation to chlorophyll estimation Journal of Plant Physiology, 143 (1994), pp. 286–292

A.A. Gitelson, Y. Peng, J.G. Masek, D.C. Rundquist, S. Verma, A. Suyker, *et al.* Remote estimation of crop gross primary production with Landsat data Remote Sensing of Environment, 121 (2012), pp. 404–414

A.A. Gitelson, A. Vina, S.B. Verma, D.C. Rundquist, T.J. Arkebauer, G. Keydan, *et al.* Relationship between gross primary production and chlorophyll content in crops: implications for the synoptic monitoring of vegetation productivity Journal of Geophysical Research, 111 (2006) D08S11

A. Harris, J. Dash The potential of the MERIS terrestrial chlorophyll index for carbon flux estimation Remote Sensing of Environment, 114 (2010), pp. 1856–1862

G. Hmimina, E. Dufrêne, J.Y. Pontailler, N. Delpierre, M. Aubinet, B. Caquet, *et al.* Evaluation of the potential of MODIS satellite data to predict vegetation phenology in different biomes: an investigation using ground-based NDVI measurements Remote Sensing of Environment, 132 (2013), pp. 145–158

A. Huete, K. Didan, T. Miura, E.P. Rodriguez, X. Gao, L.G. Ferreira Overview of the radiometric and biophysical performance of the MODIS vegetation indices Remote Sensing of Environment, 83 (2002), pp. 195–213

S. Liang, T. Zheng, R. Liu, H. Fang, S.-C. Tsay, S. Running Estimation of incident photosynthetically active radiation from moderate resolution imaging spectrometer data Journal of Geophysical Research, 111 (2006), p. D15208

R.G. Liu, S.L. Liang, H.L. He, J.Y. Liu, T. Zheng Mapping incident photosynthetically active radiation from MODIS data over China Remote Sensing of Environment, 112 (2008), pp. 998–1009

A.I. Lyapustin Interpolation and profile correction (IPC) method for shortwave radiative transfer in spectral intervals of gaseous absorption Journal of the Atmospheric Sciences, 60 (2003), pp. 865–871

G.A. Meehl, C. Tebaldi More intense, more frequent, and longer lasting heat waves in the 21st century Science, 305 (2004), pp. 994–997

L. Mercalli, D.C. Berro Atlante climatico della Valle d'Aosta. Società meteorologica subalpina (2003)

M. Meroni, A. Barducci, S. Cogliati, F. Castagnoli, M. Rossini, L. Busetto, *et al.* The hyperspectral irradiometer, a new instrument for long-term and unattended field spectroscopy measurements Review of Scientific Instruments, 82 (2011), p. 043106

M.N. Merzlyak, A. Gitelson Why and what for the leaves are yellow in autumn – on the interpretation of optical-spectra of senescing leaves (*Acer platanoides* L) Journal of Plant Physiology, 145 (1995), pp. 315–320

M. Migliavacca, M. Galvagno, E. Cremonese, M. Rossini, M. Meroni, O. Sonnentag, *et al.* Using digital repeat photography and eddy covariance data to model grassland phenology and photosynthetic CO_2 uptake Agricultural and Forest Meteorology, 151 (2011), pp. 1325–1337

J.L. Monteith Solar radiation and productivity in tropical ecosystems Journal of Applied Ecology, 9 (1972), pp. 747–766

J.L. Monteith Climate and efficiency of crop production in Britain Philosophical Transactions of the Royal Society of London. Series B, Biological Sciences, 281 (1977), pp. 271–294

C. Panigada, M. Rossini, M. Meroni, R. Marzuoli, G. Gerosa, R. Colombo Indicators of ozone effects on *Fagus sylvatica* L. by means of spectroradiometric measurements Italian Journal of Remote Sensing, 41 (2009), pp. 3–20

Y. Peng, A.A. Gitelson, G. Keydan, D.C. Rundquist, W. Moses Remote estimation of gross primary production in maize and support for a new paradigm based on total crop chlorophyll content Remote Sensing of Environment, 115 (2011), pp. 978–989

Y. Peng, A.A. Gitelson, T. Sakamoto Remote estimation of gross primary productivity in crops using MODIS 250 m data Remote Sensing of Environment, 128 (2013), pp. 186–196

M. Rossini, S. Cogliati, M. Meroni, M. Migliavacca, M. Galvagno, L. Busetto, *et al.* Remote sensing-based estimation of gross primary production in a subalpine grassland Biogeosciences, 9 (2012), pp. 2565–2584

M. Rossini, M. Meroni, M. Migliavacca, G. Manca, S. Cogliati, L. Busetto, *et al.* High resolution field spectroscopy measurements for estimating gross ecosystem production in a rice field Agricultural and Forest Meteorology, 150 (2010), pp. 1283–1296

J.W. Rouse, R.H. Haas, J.A. Schell, D.W. Deering, J.C. Harlan Monitoring the vernal advancements and retro gradation of natural vegetation NASA/GSFC Final Report, Greenbelt, MD, USA (1974), p. 371

T. Sakamoto, A.A. Gitelson, B.D. Wardlow, S.B. Verma, A.E. Suyker Estimating daily gross primary production of maize based only on MODIS WDRVI and shortwave radiation data Remote Sensing of Environment, 115 (2011), pp. 3091–3101

G. Schaepman-Strub, M.E. Schaepman, T.H. Painter, S. Dangel, J.V. Martonchik Reflectance quantities in optical remote sensing-definitions and case studies Remote Sensing of Environment, 103 (2006), pp. 27–42

D.A. Sims, J.A. Gamon Relationships between leaf pigment content and spectral reflectance across a wide range of species, leaf structures and developmental stages Remote Sensing of Environment, 81 (2002), pp. 337–354

P. Streb, W. Shang, J. Feierabend, R. Bligny Divergent strategies of photoprotection in high-mountain plants Planta, 207 (1998), pp. 313–324

C.D. Stylinski, J.A. Gamon, W.C. Oechel Seasonal patterns of reflectance indices, carotenoid pigments and photosynthesis of evergreen chaparral species Oecologia, 131 (2002), pp. 366–374

D.P. Turner, S. Urbanski, D. Bremer, S.C. Wofsy, T. Meyers, S.T. Gower, *et al.* A cross-biome comparison of daily light use efficiency for gross primary production Global Change Biology, 9 (2003), pp. 383–395

S. Wipf, C. Rixen A review of snow manipulation experiments in Arctic and alpine tundra ecosystems Polar Research, 29 (2010), pp. 95–109

C.Y. Wu, Z. Niu, Q. Tang, W.J. Huang, B. Rivard, J.L. Feng Remote estimation of gross primary production in wheat using chlorophyll-related vegetation indices Agricultural and Forest Meteorology, 149 (2009), pp. 1015–1021

C. Yi, G. Rustic, X. Xu, J. Wang, A. Dookie, S. Wei, *et al.* Climate extremes and grassland potential productivity Environmental Research Letters, 7 (2012), p. 035703